RSC Advances

PAPER

View Article Online
View Journal | View Issue

Cite this: *RSC Adv.*, 2014, **4**, 50699

Enhanced Cr(VI) removal from aqueous solutions using Ni/Fe bimetallic nanoparticles: characterization, kinetics and mechanism

Shimin Zhou,[a] Yuan Li,[b] Jitao Chen,[a] Zhongmin Liu,[a] Zhaohui Wang*[c] and Ping Na*[a]

Received 16th August 2014
Accepted 23rd September 2014

DOI: 10.1039/c4ra08754b

www.rsc.org/advances

In this study, Ni/Fe bimetallic nanoparticles were prepared by a liquid-phase chemical reduction method and characterized by scanning electron microscopy (SEM), energy dispersive X-ray spectrometry (EDS) with image mapping, transmission electron microscopy (TEM), X-ray diffraction (XRD) and X-ray photoelectron spectroscopy (XPS). The as-prepared Ni/Fe material was applied to remove Cr(VI) *via* a coupled adsorption/reduction process. It was found that Cr(VI) removal followed pseudo-second-order reaction kinetics. Acidic pH favored the efficient removal of Cr(VI) due to the abundance of reactive H$^{\bullet}$ species that were mediated by the Ni catalyst. XPS studies demonstrated that Cr(VI) removal on the surface of the bimetallic nanoparticles was a synergistic adsorption and reduction process. The introduction of nickel to nZVI not only controls iron passivation but also facilitates the efficient flow of electron transfer between iron and Cr(VI), and thus the efficient reduction of Cr(VI) to Cr(III). Hydroxylated $Cr(OH)_3$ and co-precipitation of $Cr_xFe_{1-x}(OH)_3$ were the final products of Cr(VI) removal by the Ni/Fe material.

1. Introduction

Chromium, with its significant economic importance for industrial use, is extensively applied in various industries, including electroplating, pigments, metal cleaning, leather tanning and mining.[1–3] It is one of the worst pollutants that are highly toxic to human and aquatic life.[4] Exposure to high chromium concentrations in human beings can cause health problems such as respiratory problems, cancer, skin rashes, and liver damage.[5] United States Environmental Protection Agency (USEPA) has strictly established an action level of 100 ppb for total chromium in drinking water.[6] Chromium exists in natural waters in two oxidation states, Cr(III) and Cr(VI). The Cr(VI) species chromate (CrO_4^{2-}, $HCrO_4^-$) and dichromate ($Cr_2O_7^{2-}$) are considerably mobile and soluble in aquatic environments and soil.[7,8] Cr(VI) is 500 times as toxic as Cr(III) due to its carcinogenic and mutagenic properties.[9] On the other hand, Cr(III) is recognized as an essential trace metal in human nutrition. It can be readily precipitated in the form of $Cr(OH)_3$ or adsorbed on a variety of inorganic and organic substrates under alkaline conditions.[10] Thus, it is necessary and urgent to find effective ways to remove Cr(VI) from aqueous solutions.

A number of treatment technologies, such as membrane separation, chemical precipitation, filtration, electrocoagulation, bioremediation, ion exchange and adsorption, have been developed to remove Cr(VI) from aqueous systems in recent years.[11–14] Among all these technologies, the reduction of Cr(VI) to Cr(III) followed by $Cr(OH)_3$ precipitation is known to be one of the most common and practiced approaches for Cr(VI) removal from aqueous solutions due to its low cost, easy operation and high efficiency. To date, different types of adsorbent materials have been investigated for the removal of Cr(VI) from aqueous solutions, including nano-carbonate hydroxylapatites (nano-CHAPs),[4] coir pith,[8] chitosan-coated fly ash composite,[11] activated carbonized biomass,[15] and *Helianthus annuus* stem.[16] However, all these adsorbents suffer from one or more drawbacks, limitations or scopes of application. For example, the application or treatment performance of these adsorbents is constrained by the difficulty in separating the suspension from aqueous solutions[4] and the low removal capacity after saturated adsorption.[16]

Recently, Fu and Dionysiou summarized the use of zerovalent iron for groundwater remediation and wastewater treatment in a critical review.[17] Zerovalent iron (ZVI) has attracted increasing interest for the treatment of toxic contaminants in wastewater and groundwater because ZVI, as a reductive material with standard redox potential $E^0 = -0.440$ V, is convenient and non-toxic.[18,19] In particular, previous studies have demonstrated that ZVI is an effective reductant for Cr(VI) with a standard redox potential of $E^0 = 1.33$ V under acidic conditions.[20,21] Liu *et al.*[22] demonstrated that in ZVI treatment

[a]*School of Chemical Engineering and Technology, Tianjin University, Tianjin 300072, China. E-mail: naping@tju.edu.cn; Fax: +86 22 27405967; Tel: +86 22 27405967*

[b]*Guang Dong Electric Power Design Institute, China Energy Engineering Group Co. Ltd., Guangzhou 510663, China*

[c]*College of Environmental Science and Engineering, Donghua University, Shanghai 201620, China. E-mail: zhaohuiwang@dhu.edu.cn*

systems, the removal of Cr(VI) by Fe^0 was influenced by the co-existence of humic acid and hardness in batch kinetics experiments at the initial pH of 6 and 9.5. Cr(VI) was reduced by Fe^0 and colloidal Fe–humate complexes were formed in groundwater. However, under typical environmental conditions, the removal of Cr(VI) by Fe^0 is unfavorable because of the low rate of Cr(VI) reduction. Furthermore, in the presence of water and/or oxygen, oxidation of iron metal to ferrous iron and the precipitation of iron species (α-FeOOH, γ-FeOOH, α-Fe_3O_4, $Fe(OH)_2$, $Fe(OH)_3$, and $FeCO_3$) occur on the surface of ZVI. As a result, the reduction and adsorption of Cr(VI) dramatically diminishes with time.[23] In contrast, nanoscale zerovalent iron (nZVI) particles possess the advantage of a larger reactive surface area and a higher surface reactivity, and thus a higher chemical reaction efficiency for Cr(VI) removal.[24] However, nZVI has some shortcomings in practical environmental remediation. For example, the rate of Cr(VI) reduction using nZVI is still very slow in aqueous solutions.[25] In addition, a hydroxide or oxide layer forms on the surface of nZVI during the reaction, which considerably decreases the effective use of nZVI.[9] To improve the reactivity of nZVI, a second catalytic metal, such as Pd or Ni, is often added, resulting in bimetallic Pd/Fe or Ni/Fe nanoparticles for the remediation of pollutants.[26–28] As a precious metal, Pd exhibits a better catalytic effect compared to Ni but its high cost significantly restricts its wide application. Similar to Pd, Ni as a catalyst metal has also been widely used for the removal of organic compounds in many industries.[28,29] More importantly, it has lower cost and better corrosion resistance, which makes it more suitable for wastewater treatment.[27] Bimetallic Ni/Fe nanoparticles make the nZVI more stable in air against oxidation in some cases and improve the chemical reactivity.[28] To date, the current research has mainly focused on the removal of organic chlorinated hydrocarbons and antibiotics using bimetallic nanoparticles. Little research has been demonstrated for heavy metal removal, especially for Cr(VI) removal with bimetallic nanoparticles. In particular, the removal of Cr(VI) with Ni/Fe bimetallic magnetic nanoparticles from aqueous solutions through simultaneous reduction and adsorption has not yet been studied.

Here, the aim of the present work is to examine the reactivity of Ni/Fe bimetallic nanoparticles towards Cr(VI) reduction and investigate their removal performance and mechanism. SEM, TEM, XRD and XPS measurements were used to characterize the structure of Ni/Fe bimetallic nanoparticles. In addition, other factors such as the initial pH, competitive anions, and reusability of the nanoparticles were also investigated. XPS analysis was applied to determine the predominant mechanism of Cr(VI) removal.

2. Materials and methods

2.1 Materials and reagents

All the chemicals and reagents, such as potassium dichromate ($K_2Cr_2O_7$), ferrous sulfate ($FeSO_4 \cdot 7H_2O$, AR), nickel sulfate ($NiSO_4 \cdot 7H_2O$, AR) and potassium borohydride (KBH_4, AR), were purchased from Tianjin Guangfu Fine Chemical Research Institute. All the solvents and reagents were directly used without any purification. All the solutions were prepared with deionized water (DI). All the labware used in the experiments was soaked in HNO_3 (7.5 mol L^{-1}) solution for 12 h prior to use, washed and then rinsed with deionized water. The solution pH was adjusted with HCl (0.1 mol L^{-1}) or NaOH (0.1 mol L^{-1}).

2.2 Preparation of the Ni/Fe bimetallic nanoparticles

The Ni/Fe bimetallic nanoparticles were prepared by a modified liquid-phase chemical reduction method reported by Schrick *et al.* (Fig. 1).[29] Briefly, $FeSO_4 \cdot 7H_2O$ (1.39 g) was dissolved in a 50 mL ethanol–water (4 : 1 v/v) solution, which was diverted into a three-necked open flask and mechanically stirred for 10 min. Then, a freshly prepared KBH_4 solution (1.62 g KBH_4 in 100 mL) was simultaneously added dropwise into the $FeSO_4 \cdot 7H_2O$ solution with mechanical stirring under a N_2 environment. The reaction can be described by the following equation:

$$Fe(H_2O)_6^{2+} + 2BH_4^- \rightarrow Fe^0 + 2B(OH)_3 + 7H_2 \quad (1)$$

The black solid products were separated by a magnet and washed with distilled water and ethanol several times. The freshly prepared nanoscale zerovalent iron was redispersed into 50 mL ethanol solution. Then, 0.28 g $NiSO_4 \cdot 7H_2O$ in 50 mL ethanol solution was added into the flask to achieve post-coated bimetallic nanoparticles. This process is represented by the following equation:

$$Fe^0 + Ni^{2+} \rightarrow Fe^{2+} + Ni \quad (2)$$

After 40 min, the as-obtained Ni/Fe bimetallic nanoparticles were centrifuged, washed with pure ethanol several times and dried at 70 °C for 8 h under vacuum. The nZVI was prepared by a similar procedure as described above but without the addition of Ni^{2+}. The nZVI and Ni/Fe bimetallic nanoparticles were stored in sealed brown bottles and kept in a N_2 atmosphere prior to use.

2.3 Characterization of the Ni/Fe bimetallic nanoparticles

The morphology of the samples was scanned by a Hitachi S-4800 scanning electron microscope (SEM) operating at 15 kV. Transmission electron microscope (TEM) images were recorded on a Tecnai G2 F20 microscope (PANalytical, Netherlands) operating at 100 kV. X-ray diffraction (XRD) experiments were carried out in a PANalytical X-ray diffractometer (PANalytical

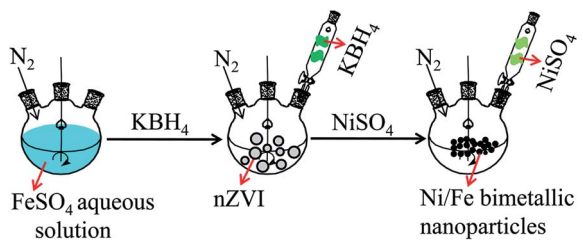

Fig. 1 Schematic diagram for the preparation of Ni/Fe bimetallic nanoparticles by the liquid-phase chemical reduction method.

Corporation, X'Pert, Netherlands) with Co Kα radiation (λ = 0.154 nm) at 45 kV/40 mA. X-ray photoelectron spectroscopy (XPS, Perkin-Elmer Corporation, USA) was performed on a Physical Electronics PHI 1600 X-ray photoelectron spectrometer using 300 W Mg Kα radiation.

2.4 Batch experiments

A stock solution of Cr(VI) (100 mg L^{-1}) was prepared by dissolving potassium dichromate in deionized distilled water. Batch experiments examined the removal of Cr(VI) from aqueous solutions using Ni/Fe bimetallic nanoparticles. Cr(VI) removal experiments were carried out on a constant temperature shaker (HZ-9511K) at 200 rpm and 25 °C in a 250 mL conical flask, which contained 100 mL Cr(VI) solution. At various time intervals, approximately 2 mL samples were withdrawn using a 3 mL plastic syringe from the reaction mixture. To study the effect of pH on the removal of Cr(VI) by Ni/Fe bimetallic nanoparticles, experiments were conducted using 100 mL Cr(VI) solution with an initial concentration of 25 mg L^{-1} and 0.1 g adsorbent in the pH range 2.0–7.0 for 150 min. The sample solutions were filtered through a 0.22 μm membrane filter. Then, Cr(VI) concentration was determined using the 1,5-diphenylcarbazide colorimetric method[30] at 540 nm on a UV-vis spectrophotometer (Perkin Elmer, Lambda-35). The total Cr concentration in the solution was measured by atomic absorption spectroscopy (AAS, Hitachi Z-5300) with a detection limit of 0.02 μg L^{-1}. The removal of Cr(VI) was calculated according to the following mass balance eqn (3) and (4):

$$q_e = \frac{(C_0 - C_e)V}{m} \quad (3)$$

$$\text{Removal efficiency } (\%) = \frac{C_0 - C_e}{C_0} \times 100\% \quad (4)$$

where q_e (mg g^{-1}) is the equilibrium adsorption capacity, C_0 and C_e are the initial and equilibrium concentrations of Cr(VI) in solution (mg L^{-1}), respectively, V is the volume of aqueous solutions (L) and m is the amount of the adsorbent (g).

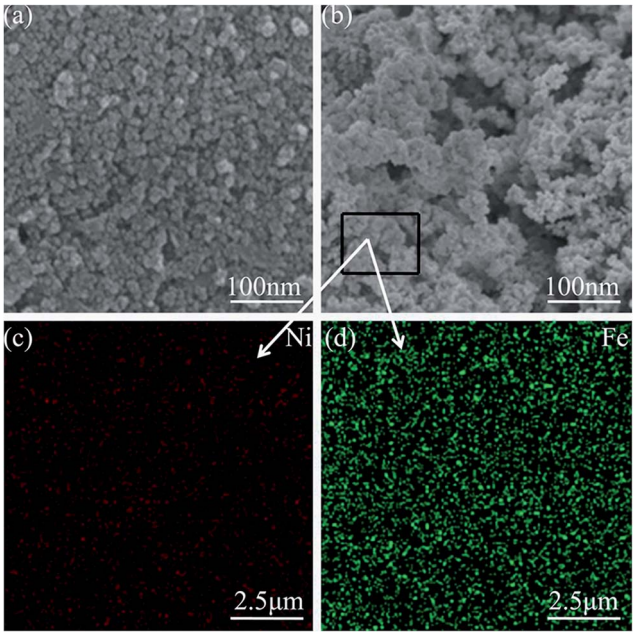

Fig. 2 SEM micrograph of (a) nZVI and (b) Ni/Fe bimetallic nanoparticles, as well as the EDS (c) Ni mapping and (d) Fe mapping for the Ni/Fe bimetallic nanoparticles.

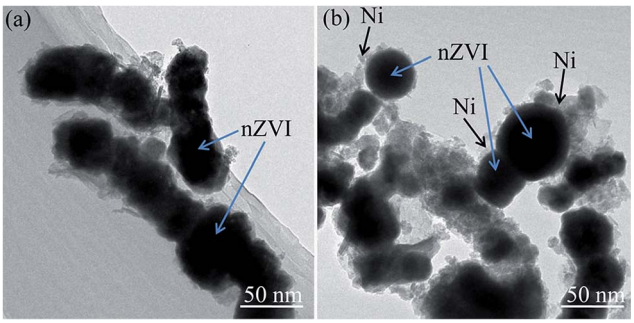

Fig. 3 TEM images of (a) nZVI and (b) Ni/Fe nanoparticles.

3. Results and discussion

3.1 Characterization of the Ni/Fe bimetallic nanoparticles

Fig. 2 shows the SEM images of the as-prepared nZVI and the Ni/Fe bimetallic nanoparticles, as well as the EDS mapping for the Ni/Fe bimetallic nanoparticles. The morphology of Fe nanoparticles was found to be mostly spherical in shape (30–60 nm) and they existed as prominent aggregates in Fig. 2a. As shown in Fig. 2b, Ni particles were mainly dispersed on the nZVI surface. Because of magnetic and electronic interactions between the metals,[31] the as-prepared products were aggregated and uniformly spherical with the average grain sizes of approximately 50 nm. To further determine the distribution of Fe and Ni, SEM-EDS mapping was employed to characterize the Ni/Fe bimetallic nanoparticles. As shown in Fig. 2c and d, Ni particles were dispersed homogeneously into the Fe phase.

Fig. 3 shows the TEM images of nZVI and Ni/Fe bimetallic nanoparticles. The necklace-like aggregates of bare nZVI particles were observed in Fig. 3a. The average diameter of nZVI (Fig. 3a) and Ni/Fe nanoparticles (Fig. 3b) was about 30–60 nm. As shown in Fig. 3b, Ni particles located on the surface of the nZVI were also observed. Fig. 4 shows the XRD patterns of the as-prepared nZVI and the Ni/Fe bimetallic nanoparticles, where large diffraction peaks were accompanied with some small peaks. XRD analysis of the nZVI (Fig. 4a) indicates that the nZVI prepared by the liquid-phase chemical reduction method had a diffraction peak centered at 44.7° for the (110) facet of bcc iron, which could be assigned to a cubic phase of iron (JCPDS field card no. 06-0696). Other satellite peaks in the range 30–40° revealed the formation of oxides on the surface of the nZVI.[32] In Fig. 4b, the diffraction peaks at 2θ 44.75° and 64.94° correspond to the (110) and (200) crystal planes of the body centered cubic (bcc) Ni–Fe alloy (JCPDS 37-0474), respectively, which is consistent with the previously reported Ni/Fe nanoparticles.[33] Compared with nZVI, the surface of the Ni/Fe bimetallic nanoparticles was devoid of oxide peaks in the range 30–40°,

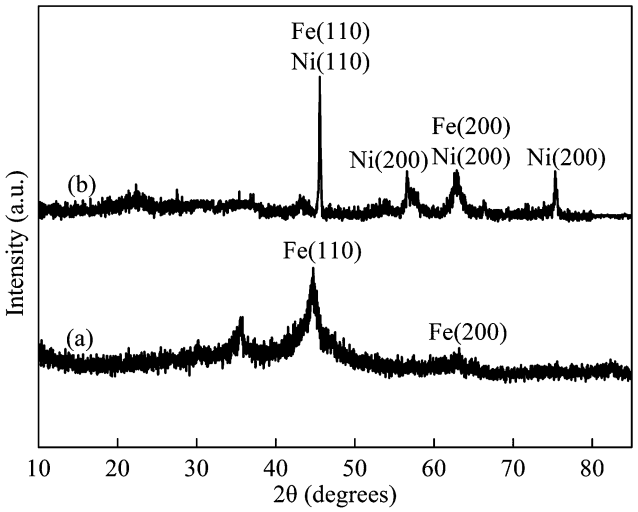

Fig. 4 XRD patterns of (a) nZVI and (b) the as-prepared Ni/Fe nanoparticles.

implying the anticorrosion effect of the coated Ni on the surface property of nZVI.

XPS analysis of the as-synthesized Ni/Fe bimetallic nanoparticles was conducted to elucidate the surface state of the sample in Fig. 5. The wide-scan XPS spectrum of the Ni/Fe bimetallic nanoparticles composites (Fig. 5a) shows that C, O, Fe, and Ni were present on the surface of the as-prepared Ni/Fe nanoparticles. As shown in Fig. 5b, the characteristic peaks of Fe^0 appeared at 706.9 eV (Fe $2p_{3/2}$) and 719.8 eV (Fe $2p_{1/2}$), respectively, while broad peaks at 710.8 eV and 724.5 eV were attributed to iron oxides.[34] In addition, the Ni 2p spectrum of the Ni/Fe bimetallic nanoparticles presented three peaks with the binding energies of 852.3, 855.8 and 878.7 eV *via* deconvolution (Fig. 5c), which could be assigned to the characteristic features of Ni^0, Ni^{2+} ($2p_{3/2}$) and Ni^{2+} ($2p_{1/2}$), respectively.[35] Therefore, XPS further confirmed the surface chemical composition of Ni/Fe nanoparticles.

3.2 Effect of initial pH

The pH of the aqueous solution is one of the most important parameters in Cr(VI) removal. Solution pH can affect species distribution and the rate of Cr(VI) removal. It was observed that hydroxide and oxide layers were easily formed on the surface of iron nanoparticles under alkaline conditions, which impeded the removal of Cr(VI) by iron nanoparticles.[36,37] Therefore, we examined the effect of pH on the removal of Cr(VI) by nZVI and Ni/Fe bimetallic nanoparticles in the pH range of 2.0–7.0 (Fig. 6). The removal efficiency of Cr(VI) by Ni/Fe bimetallic nanoparticles was the highest at pH 2. With the increase in pH, Cr(VI) removal by bimetallic nanoparticles decreased from 96.33% at pH 2.0 to 60.31% at pH 7.0. It could be because an amount of toxic Cr(VI) was reduced to the less toxic Cr(III), which was attributed to the reactive $H^{\cdot}$ species that were catalyzed by Ni, and thus further formed Cr–Fe complexes. A possible mechanism for this reduction is proposed in eqn (5)–(9):

$$Fe - Ni + H^+ \rightarrow Fe^+ - Ni + H^{\cdot} \quad (5)$$

$$Fe^+ - Ni + H^+ \rightarrow Fe^{2+} - Ni + H^{\cdot} \quad (6)$$

$$Fe^{2+} - Ni \rightarrow Fe - Ni^{2+} \quad (7)$$

$$3H^{\cdot} + Cr(VI) \rightarrow Cr(III) + 3H^+ \quad (8)$$

$$xCr(III) + (1 - x)Fe(III) + 2H_2O \rightarrow Cr_xFe_{1-x}OOH + 3H^+ \quad (9)$$

Compared with nZVI, Ni/Fe bimetallic nanoparticles were efficient for Cr(VI) removal in the pH range 2.0–7.0. This could be due to the enhanced efficient flow of electron transfer between iron and Cr(VI) by the introduction of nickel, thus lowering the concentration of Cr(VI) in the solution. At pH < 7.0, Cr(VI) speciation is predominantly $HCrO_4^-$. As the pH decreased, Cr(VI) can be more easily reduced.[2] The yield of reactive $H^{\cdot}$ species was also increased *via* nickel hydride formation with the increase in $[H^+]$. Therefore, the removal efficiency of Cr(VI) by Ni/Fe bimetallic nanoparticles was enhanced. Considering the removal efficiency and the feasibility of actual operation, an initial pH of 3.0 was used as the optimum pH in the following experiments. Meanwhile, we measured the dissolved Fe and Ni concentrations in solution at different initial pH values. The concentration of Fe ions decreased from 1.30 to 0.25 mg L^{-1} as pH increased from 2.0 to 7.0. However, the concentration of Ni ions was about 0.20 mg L^{-1}, which showed no obvious change with the increase in initial pH. The mass ratios of dissolved Fe and Ni in the bimetal are 0.13% and 0.02%, respectively. Therefore, it was shown that there was no significant Ni^{2+} or Fe^{2+}/Fe^{3+} dissolved into solution.

3.3 Effect of contact time and adsorption kinetics

The kinetics for Cr(VI) removal by nZVI and Ni/Fe bimetallic nanoparticles are shown in Fig. 7. It is clear that Cr(VI) removal efficiency increased markedly with increasing contact time during the initial 20 min of equilibration time. Subsequently, a slight fluctuation occurred and an apparent equilibrium was achieved after about 150 min. At the beginning, rapid removal is attributed to the greater concentration gradient and more available sites for Cr(VI) adsorption by bimetallic nanoparticles. The removal efficiency was obviously improved after the introduction of Ni. More than 90% of Cr(VI) ions were removed by Ni/Fe bimetallic nanoparticles, while only about 70% of Cr(VI) ions were removed by nZVI. In comparison to nZVI particles with Cr(VI), the active sites present in the bimetallic Ni/Fe nanoparticles are the catalytic Ni, which act as electron shuttle between donors and acceptors and play an important role in increasing the reduction activity. This result was similar to the reported paper for Ni–Fe bimetal with high dechlorination activity for 4-chlorophenol.[38] It could still be found that the Cr(III) concentration in solution was very low as compared with the initial Cr(VI) concentration after Cr(VI) was removed by Ni/Fe bimetallic nanoparticles and nZVI, respectively.

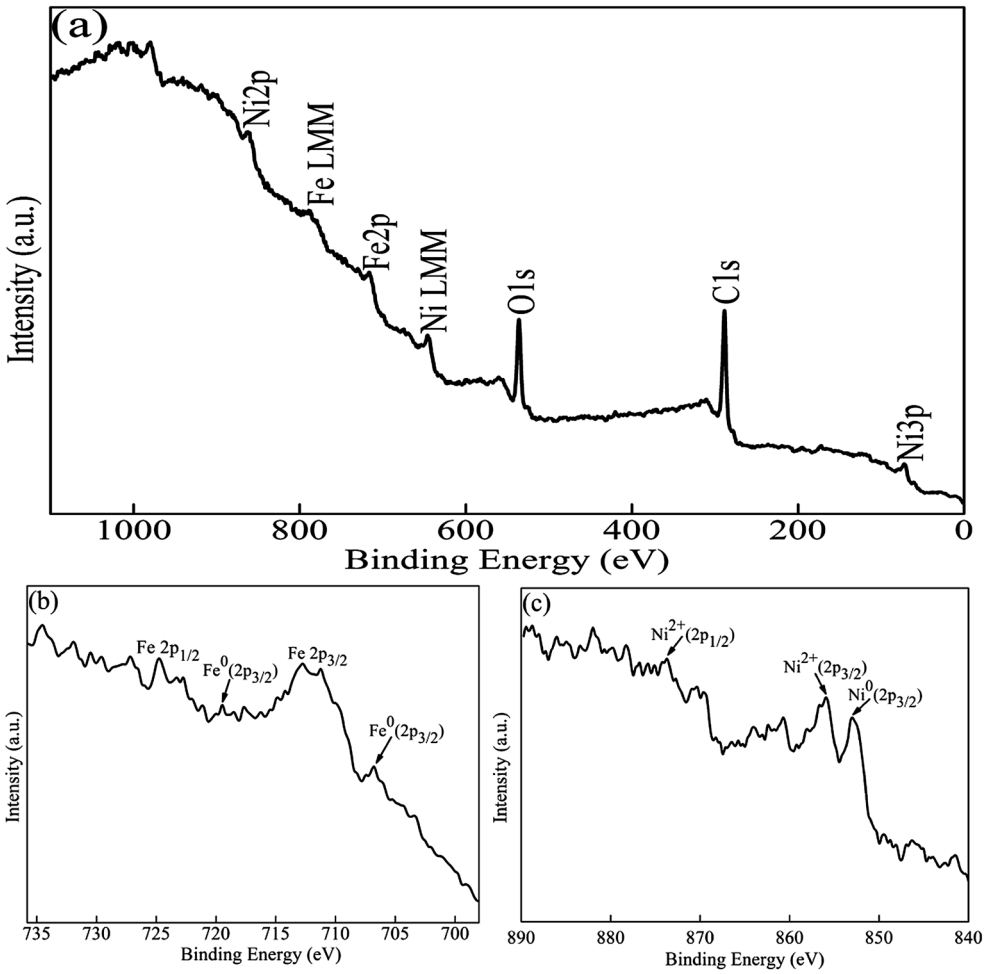

Fig. 5 XPS spectra of the Ni/Fe bimetallic nanoparticles: (a) wide scan, (b) Fe 2p spectrum, (c) Ni 2p spectrum.

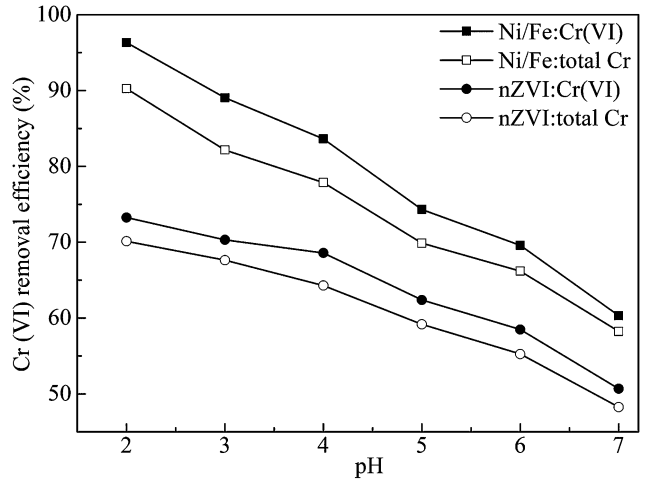

Fig. 6 Effect of pH values on total Cr(VI) and Cr(VI) removal by nZVI and Ni/Fe bimetallic nanoparticles ($[Cr(VI)]_0 = 25$ mg L^{-1}, adsorbent = 1.0 g L^{-1}, time = 150 min).

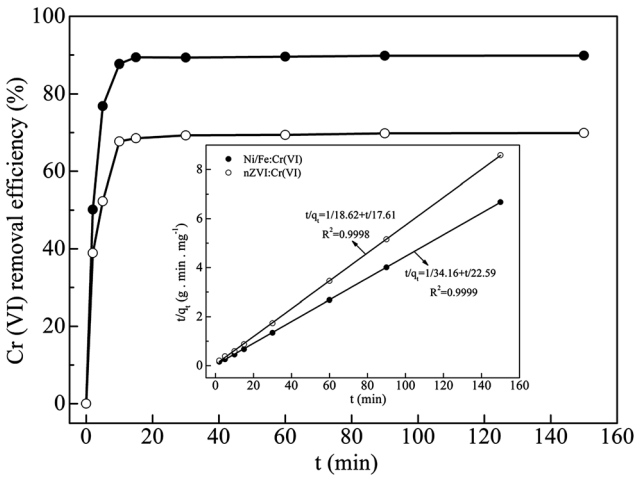

Fig. 7 Kinetics of Cr(VI) removal and pseudo-second order kinetic of Cr(VI) adsorption (inset) by nZVI and Ni/Fe bimetallic nanoparticles ($[Cr(VI)]_0 = 25$ mg L^{-1}, adsorbent = 1 g L^{-1}, pH = 3.0 and $t = 150$ min).

To further understand the kinetics, the pseudo-second-order kinetic model was employed to describe the kinetic characteristics of the adsorption/reduction of Cr(VI) by nZVI and Ni/Fe bimetallic nanoparticles. The pseudo-second-order model can be expressed as follows:[39]

$$\frac{dq_t}{dt} = k_2(q_e - q_t)^2 \quad (10)$$

$$\frac{t}{q_t} = \frac{1}{k_2 q_t^2} + \frac{t}{q_e} \quad (11)$$

where q_t (mg g^{-1}) is the amount of Cr adsorbed at time t (min) and q_e (mg g^{-1}) is the amount of adsorption at equilibrium. k_2 (mg g^{-1} min^{-1}) is the pseudo-second-order reaction rate. The parameters k_2 and q_e can be estimated from the intercept and slope of the (t/q_t) *vs.* t plot, respectively. The model parameters and equilibrium concentrations obtained from both the models are listed in Table 1. As shown in Fig. 7 (inset), the linear relationships show very high correlation coefficients $R^2 > 0.999$, demonstrating that the pseudo-second-order model well described the removal kinetics of Cr(VI).

3.4 Effects of competitive anions

To evaluate the selectivity of Ni/Fe bimetallic nanoparticles, the effects of four competitive anions, including Cl^-, NO_3^-, SO_4^{2-} and PO_4^{3-}, on Cr(VI) removal were also evaluated (Fig. 8). When the concentrations of Cl^- and NO_3^- ranged from 100 to 400 mg L^{-1}, the removal efficiency of Cr(VI) did not show an obvious change in aqueous solutions. However, the presence of SO_4^{2-} and PO_4^{3-} could reduce the capacity of removing Cr(VI) by 16.4% and 26.0%, respectively. Cl^- and NO_3^- are monovalent anions, and have weak competition for the adsorption sites of bimetallic nanoparticles. The multivalent anions, SO_4^{2-} and PO_4^{3-}, have similar structures and sizes as $HCrO_4^-$ and $Cr_2O_7^{2-}$. They could compete with Cr(VI) for the available adsorption sites of bimetallic nanoparticles. Thus, with an increase in the concentrations of SO_4^{2-} and PO_4^{3-}, the Cr(VI) removal reduced gradually.

3.5 XPS analysis

To find out the main mechanisms of Cr(VI) removal by Ni/Fe bimetallic nanoparticles and the change in the valence states of the chemical elements, X-ray photoelectron spectroscopy (XPS) was carried out to study the surface chemical compositions of the materials obtained before and after their treatment with chromium solution, and the results are presented in Fig. 9.

Table 1 Pseudo-second-order model parameters for Cr(VI) removal by nZVI and Ni/Fe bimetallic nanoparticles

	Cr(VI) removal		
Adsorbents	q_e (mg g^{-1})	k (g mg^{-1} min^{-1})	R^2
Ni/Fe	22.59	0.0669	0.9999
nZVI	17.61	0.0600	0.9998

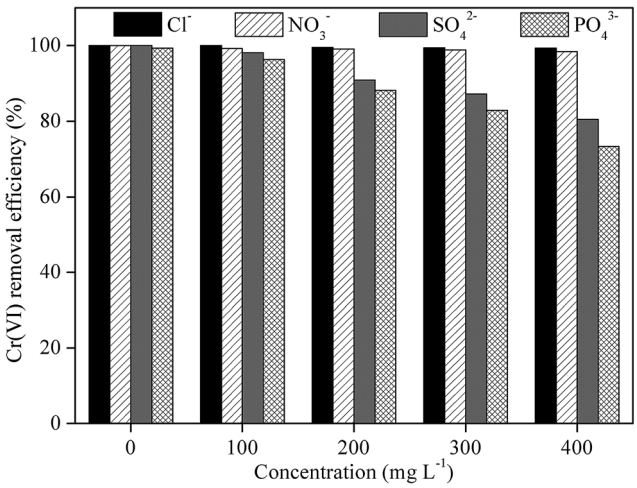

Fig. 8 Effect of different competitive anions concentration of Cl^-, NO_3^-, SO_4^{2-}, and PO_4^{3-} on Cr(VI) removal by Ni/Fe bimetallic nanoparticles ($[Cr(VI)]_0 = 25$ mg L^{-1}, adsorbent = 1g L^{-1}, pH = 3.0 and $t = 150$ min).

As shown in Fig. 9a, the whole-region scan of the Ni/Fe bimetallic nanoparticles surface before and after being exposed to the aqueous solution containing 50 mg L^{-1} Cr(VI) at an initial pH of 3 and 20 °C. Compared with the freshly prepared Ni/Fe bimetallic nanoparticles (Fig. 9a(i)), a new Cr peak at about 580 eV (Fig. 9a(ii)) appeared after contact with Cr(VI) for 150 min, indicating the uptake of chromium on the Ni/Fe bimetallic nanoparticles surface.

Detailed XPS surveys of the regions for Cr 2p are shown in Fig. 9b. The photoelectron peaks for Cr $2p_{3/2}$ and $2p_{1/2}$ centered at 577.0 and 586.8 eV, respectively, indicate that Cr(III) was the predominant chromium species on the surface.[40] These data demonstrates that part of the adsorbed Cr(VI) anions were reduced to Cr(III) after exposure to Ni/Fe bimetallic nanoparticles. After the deconvolution using Gaussian–Lorentz fitting, the Cr $2p_{3/2}$ photoelectron peaks at 577.1 and 577.3 eV represent the formation of $Cr(OH)_3$ on the surface of Ni/Fe bimetallic nanoparticles. The Cr $2p_{1/2}$ photoelectron peak at 586.2 eV represents Cr_2O_3. The Cr $2p_{3/2}$ and Cr $2p_{1/2}$ photoelectron peaks at 576.2 and 587.6 eV indicate the presence of other Cr(III) compounds, such as $Cr_xFe_{1-x}(OH)_3$, on the Ni/Fe nanoparticles surface.[41] Li *et al.* also found that Cr(III) was subsequently precipitated as Cr–Fe hydroxides with a representative formula approximating to $Cr_{0.67}Fe_{0.33}(OH)_3$ on the surface of bare Fe^0 nanoparticles.[42] However, there were no obvious bands of Cr(VI) in the XPS spectrum of Ni/Fe bimetallic nanoparticles after contact with Cr(VI) solution, which was consistent with the previous study.[43] The Cr(VI) removal process involved the reduction of Cr(VI) into Cr(III), and consequently either adsorption or co-precipitation of reduction products, such as $Cr(OH)_3$, Cr_2O_3 and co-precipitation of $Cr_xFe_{1-x}(OH)_3$.

There were two dominant peaks for Fe 2p (11.39%) at 711 and 725 eV, which could be assigned to Fe_3O_4 and Fe_2O_3 in Fig. 9c, respectively, according to previous studies.[44] The satellite shown between the two dominant peaks was contributed by

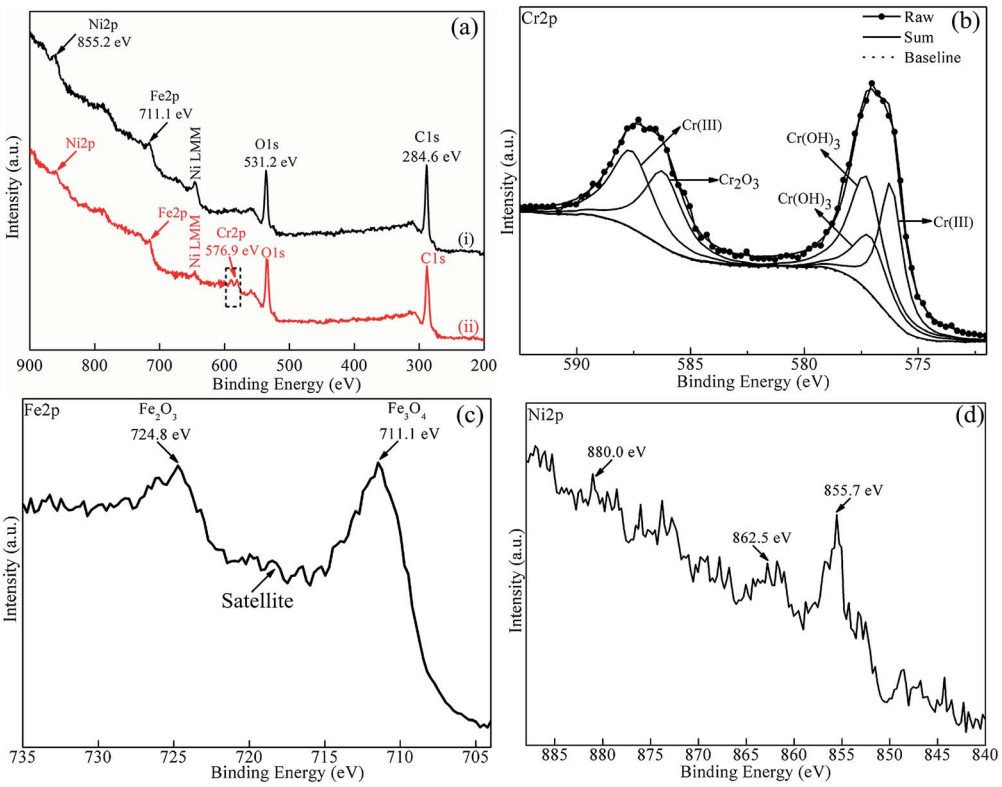

Fig. 9 (a) XPS wide survey for Ni/Fe bimetallic nanoparticles before (i) and after (ii) Cr(VI) removal, XPS survey of (b) Cr 2p, (c) Fe 2p and (d) Ni 2p of Ni/Fe bimetallic nanoparticles after Cr removal.

Fe^{2+} *via* a shake-up process.[45] As indicated in Fig. 9c, there was almost no peak corresponding to Fe^0, which might be because extensive oxidation of iron occurred on the surface of the Ni/Fe bimetallic nanoparticles. For Ni 2p, the striking feature of the XPS spectrum of reused nanoparticles is the presence of peaks at 855.7 and 862.5 eV (Fig. 9d), characteristic of Ni $2p_{3/2}$ and Ni $2p_{1/2}$, respectively. The appearance of two strong satellite features, corresponding to Ni $2p_{3/2}$ (862.2 eV) and Ni $2p_{1/2}$ (880.0 eV) signals indicated the presence of electron correlation in the system.[43] This result reveals the presence of predominantly Ni^{2+} species with satellite peaks on the bimetallic nanoparticles surface.

3.6 Mechanism of Cr(VI) removal by Ni/Fe bimetallic nanoparticles

A plausible mechanism (Fig. 10) is proposed to clearly describe the entire process of Cr(VI) removal on the Ni/Fe bimetallic nanoparticles surface as follows:

(1) Adsorption of Cr(VI) by iron oxide on the surface of Ni/Fe bimetallic nanoparticles, as summarized in reaction (12):

$$\mathrm{Cr(VI)(aq.)} + \mathrm{Fe_2O_3(Fe_3O_4)} \rightarrow \mathrm{Cr(VI)} - \mathrm{Fe_2O_3(Fe_3O_4)\ (adsorption)} \quad (12)$$

(2) Reduction of Cr(VI) to Cr(III) by reactive H˙ species catalyzed by Ni,[46,47] this process can be summarized by reactions (5)–(8) in the discussion section.

(3) Cr(III) adsorbed on the surface of iron oxide accompanied with the formation of hydroxylated $Cr(OH)_3$ and co-precipitation of $Cr_xFe_{1-x}(OH)_3$. This process can be summarized by reactions (13)–(15):

$$\mathrm{Cr(III)(aq.)} + \mathrm{Fe_2O_3(Fe_3O_4)} \rightarrow \mathrm{Cr(III)} - \mathrm{Fe_2O_3(Fe_3O_4)\ (adsorption)} \quad (13)$$

$$\mathrm{Cr(III)} + 3\mathrm{H_2O} \rightarrow \mathrm{Cr(OH)_3} + 3\mathrm{H^+}\ \mathrm{(precipitation)} \quad (14)$$

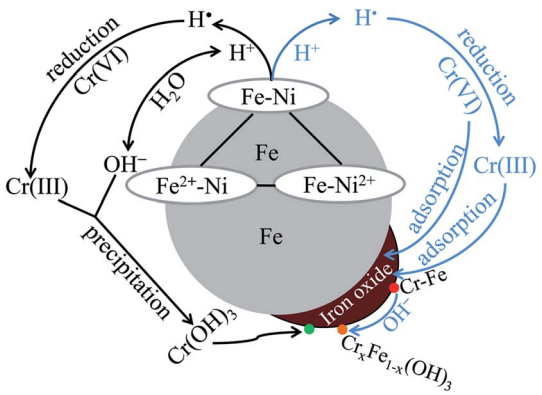

Fig. 10 Schematic representation of mechanistic pathway for Cr(VI) removal by Ni/Fe bimetallic nanoparticles.

$$x\mathrm{Cr}^{3+} + (1 - x)\mathrm{Fe}^{3+} + 3\mathrm{H_2O} \rightarrow \mathrm{Cr}_x\mathrm{Fe}_{1-x}(\mathrm{OH})_3 + 3\mathrm{H}^+ \text{ (co-precipitation)} \quad (15)$$

In such a scenario, reduction and adsorption of Cr(VI) simultaneously occur on the composite surface. The presence of a nickel catalyst in the Ni/Fe nanoparticles is shown to not only inhibit iron passivation but also facilitate the efficient flow of electron transfer from iron (donor) to Cr(VI) (acceptor) mediated by the Ni site that acts as an electron shuttle between the donor and acceptor. This adsorptive reduction process is found to be a facile electron transfer from the Ni/Fe nanoparticle to the adsorbed Cr(VI) species that results in efficiently reducing Cr(VI) to Cr(III).

4. Conclusions

In this work, Ni/Fe bimetallic nanoparticles were successfully synthesized and applied to remove Cr(VI) from aqueous solutions. The prepared Ni/Fe nanoparticles demonstrated better treatment performance for Cr(VI) removal at acidic pH due to an increase in reactive H^* species that was mediated by the Ni catalyst with the increase in $[H^+]$. The pseudo-second-order kinetics could describe the experimental data well. The presence of Cl^- and NO_3^- (up to 400 mg L^{-1}) did not affect the removal efficiency (>98%) of Cr(VI) by Ni/Fe nanoparticles, while multivalent anions (SO_4^{2-} and PO_4^{3-}) could hinder the Cr(VI) adsorption. XPS analysis confirmed that Cr_2O_3, $Cr(OH)_3$ and Cr(III) compounds existed on the surface of Ni/Fe nanoparticles. Therefore, this study provides an alternative efficient technology to simultaneously reduce and immobilize Cr pollutants.

Acknowledgements

This study is supported by the National High Technology Research and Development Program of China (863 Program) (no. 2012AA063504), the National Natural Science Foundation of China (no. 21276193), Tianjin Municipal Natural Science Foundation (no. 2013F1-0033), and Project of Ocean with Scientific Technology in Tianjin (no. KJXH2011-10).

References

1 P. R. Wittbrodt and C. D. Palmer, *Environ. Sci. Technol.*, 1995, **29**, 255–263.
2 Z. H. Wang, R. T. Bush, L. A. Sullivan and J. S. Liu, *Environ. Sci. Technol.*, 2013, **47**, 6486–6492.
3 W. J. Jiang, M. Pelaez, D. D. Dionysiou, M. H. Entezari, D. Tsoutsou and K. O'Shea, *Chem. Eng. J.*, 2013, **222**, 527–533.
4 W. Q. Tang, R. Y. Zeng, Y. L. Feng, X. M. Li and W. Zhen, *Chem. Eng. J.*, 2013, **222**, 340–346.
5 W. J. Jiang, Q. Cai, W. Xu, M. W. Yang, Y. Cai, D. D. Dionysiou and K. E. O'Shea, Cr(vi) Adsorption and Reduction by Humic Acid Coated on Magnetite, *Environ. Sci. Technol.*, 2014, **48**, 8078–8085.
6 B. Qiu, C. X. Xu, D. Z. Sun, H. G. Wei, X. Zhang, J. Guo, Q. Wang, D. Rutman, Z. H. Guo and S. Y. Wei, *RSC Adv.*, 2014, **4**, 29855–29865.
7 H. B. Gu, S. B. Rapole, J. Sharma, Y. D. Huang, D. M. Cao, H. A. Colorado, Z. P. Luo, N. Haldolaarachchige, D. P. Young, B. Walters, S. Y. Wei and Z. H. Guo, *RSC Adv.*, 2012, **2**, 11007–11018.
8 P. Suksabye, A. Nakajima, P. Thiravetyan, Y. Baba and W. Nakbanpote, *J. Hazard. Mater.*, 2009, **161**, 1103–1108.
9 X. J. Wang, J. R. Wang, L. L. Chang, Q. Ding, H. L. Liu and X. Y. Jiang, *RSC Adv.*, 2012, **2**, 12315–12321.
10 Y. Chen, H. Xu, S. Y. Wang and L. Kang, *RSC Adv.*, 2014, **4**, 17805–17811.
11 Y. Wen, Z. R. Tang, Y. Chen and Y. X. Gu, *Chem. Eng. J.*, 2011, **175**, 110–116.
12 M. Owlad, M. K. Aroua, W. A. W. Daud and S. Baroutian, *Water, Air, Soil Pollut.*, 2009, **200**, 59–77.
13 T. Kurniawan, G. Chan, W. Lo and S. Babel, *Chem. Eng. J.*, 2006, **118**, 83–98.
14 A. K. Golder, A. K. Chanda, A. N. Samanta and S. Ray, *Sep. Purif. Technol.*, 2011, **76**, 345–350.
15 S. S. Baral, S. N. Das, G. R. Chaudhury, Y. V. Swamy and P. Rath, *Chem. Eng. J.*, 2008, **139**, 245–255.
16 M. Jain, V. K. Garg and K. Kadirvelu, *J. Hazard. Mater.*, 2009, **162**, 365–372.
17 F. L. Fu, D. D. Dionysiou and H. Liu, *J. Hazard. Mater.*, 2014, **267**, 194–205.
18 W. L. Yan, H. L. Lien, B. E. Koel and W. X. Zhang, *Environ. Sci.: Processes Impacts*, 2013, **15**, 63–77.
19 P. Mitra, D. Sarkara, S. Chakrabartia and B. K. Dutta, *Chem. Eng. J.*, 2012, **171**, 54–60.
20 K. C. K. Lai and I. M. C. Lo, *Environ. Sci. Technol.*, 2008, **42**, 1238–1244.
21 R. T. Wilkin, C. M. Su, R. G. Ford and C. J. Paul, *Environ. Sci. Technol.*, 2005, **39**, 4599–4605.
22 T. Liu, D. C. W. Tsang and I. M. C. Lo, *Environ. Sci. Technol.*, 2008, **42**, 2092–2098.
23 M. Rivero-Huguet and W. D. Marshall, *J. Hazard. Mater.*, 2009, **169**, 1081–1087.
24 T. Liu, Z. Wang, L. Zhao and X. Yang, *Chem. Eng. J.*, 2012, **189–190**, 196–202.
25 H. S. Cao and W. X. Zhang, *J. Hazard. Mater.*, 2006, **132**, 213–219.
26 L. Li, M. H. Fan, R. Brown, J. H. Van Leeuwen, J. J. Wang, W. H. Wang, Y. H. Song and P. Y. Zhang, *Crit. Rev. Environ. Sci. Technol.*, 2006, **36**, 405–431.
27 Z. Zhang, N. M. Cissoko, J. J. Wo and X. H. Xu, *J. Hazard. Mater.*, 2009, **165**, 78–86.
28 X. L. Weng, S. Lin, Y. H. Zhong and Z. L. Chen, *Chem. Eng. J.*, 2013, **229**, 27–34.
29 B. Schrick, J. L. Blough, A. D. Jones and T. E. Mallouk, *Chem. Mater.*, 2002, **14**, 5140–5147.
30 Y. Lan, B. Deng, C. Kim, E. C. Thornton and H. Xu, *Environ. Sci. Technol.*, 2005, **39**, 2087–2094.
31 A. D. Bokare, R. C. Chikate, C. V. Rode and K. M. Paknikar, *Environ. Sci. Technol.*, 2007, **41**, 7437–7443.
32 X. Zhang, S. Lin, Z. L. Chen, M. Megharaj and R. Naidu, *Water Res.*, 2011, **45**, 3481–3488.
33 M. Dickinson, T. B. Scott, R. A. Crane, O. Riba, R. J. Barnes and G. M. Hughes, *J. Nanopart. Res.*, 2010, **12**, 2081–2092.

34 J. Su, S. Lin, Z. L. Chen, M. Megharaj and R. Naidu, *Desalination*, 2011, **280**, 167–173.
35 Z. Q. Fang, X. H. Qiu, J. H. Chen and X. Q. Qiu, *J. Hazard. Mater.*, 2011, **185**, 958–969.
36 M. J. Alowitz and M. M. Scherer, *Environ. Sci. Technol.*, 2002, **36**, 299–306.
37 J. Hu, G. H. Chen and I. M. C. Lo, *Water Res.*, 2009, **43**, 3067–3075.
38 F. Y. Xu, S. B. Deng, J. Xu, W. Zhang, M. Wu, B. Wang, J. Huang and G. Yu, *Environ. Sci. Technol.*, 2012, **46**, 4576–4582.
39 S. M. Zhou, D. Wang, H. Y. Sun, J. T. Chen, S. H. Wu and P. Na, *Water, Air, Soil Pollut.*, 2014, **225**, 1945–1956.
40 N. Fiol, C. Escudero and L. Villaescusa, *Bioresour. Technol.*, 2008, **99**, 5030–5036.
41 B. A. Manning, J. R. Kiser, H. Kwon and S. R. Kanels, *Environ. Sci. Technol.*, 2007, **41**, 586–592.
42 X. Q. Li, J. Cao and W. X. Zhang, *Ind. Eng. Chem. Res.*, 2008, **47**, 2131–2139.
43 A. D. Bokare, R. C. Chikate, C. V. Rode and K. M. Paknikar, *Appl. Catal., B*, 2008, **79**, 270–278.
44 P. P. Huang, Z. F. Ye, W. M. Xie, Q. Chen, J. Li, Z. C. Xu and M. S. Yao, *Water Res.*, 2013, **47**, 4050–4058.
45 K. Volgmann, F. Voigts and W. Maus-Friedrichs, *Surf. Sci.*, 2010, **604**, 906–913.
46 D. R. Petkar, B. S. Kadu and R. C. Chikate, *RSC Adv.*, 2014, **4**, 8004–8010.
47 W. H. Zhang, X. Quan and Z. Y. Zhang, *J. Environ. Sci.*, 2007, **19**, 362–366.